Research Article

Rehman Ullah, Sumaira Shah*, Zahir Muhammad, Sajjad Ali Shah, Shah Faisal, Umbreen Khattak, Tauheed ul Haq, and Muhammad Taj Akbar

In vitro and *in vivo* applications of *Euphorbia wallichii* shoot extract-mediated gold nanospheres

https://doi.org/10.1515/gps-2021-0013
received January 06, 2021; accepted January 26, 2021

Abstract: The current study was designed to investigate the potential of *Euphorbia wallichii* shoot extract for reducting Au^{3+} and stabilizing gold nanoparticles. UV-visible spectra of gold nanoparticles showed obvious surface plasmon resonance peak at 548 nm. Microscopy (SEM and TEM) showed spherical dimensions, and the energy dispersive X-ray spectra displayed the strongest optical absorption peak for gold (Au) at 2.1 keV. Dynamic light scattering spectra represent polydispersed mixture with particulate diameter of 2.5–103.2 nm. The IR spectra confirm the potential functional groups of shoot extract responsible for the reduction of Au^{3+} to gold nanoparticles which exhibit tremendous antibacterial potential of 76.31%, 68.47%, 79.85%, 48.10%, and 65.53% against *Escherichia coli*, *Staphylococcus aureus*, *Bacillus pumilus*, *Pseudomonas aeruginosa*, and *Klebsiella pneumoniae*, respectively. Gold nanoparticles showed markedly elevated fungicidal potency compared to the shoot extract alone against the tested fungal strains. IC_{50} for 2,2-diphenyl-1-picrylhydrazyl scavenging was 31.52, 18.29, and 15.32 µg/mL at 30, 60, and 90 min of reaction time, respectively. Both shoot extract and nanoparticles revealed 71% mortality at 100 µg/mL, with LD_{90} values of 310.56 µg/mL. Experimental mice acquired dose-dependent analgesia of 54.21%, 82.60%, and 86.53% when treated with gold nanoparticles at 50, 100, and 200 mg/kg bw. Inhibition of gastrointestinal muscular contraction was 21.16%, 30.49%, and 40.19% in mice feed with 50, 100, and 200 mg/kg bw, respectively.

Keywords: *Euphorbia wallichii*, gold nanospheres, characterization, *in vitro*, *in vivo* applications

1 Introduction

Centuries ago, gold nanoparticles (AuNPs) have been utilized by artists due to its interaction with light and capability to produce attractive colors. Besides, biomedical and electrical engineers are also taking advantages of the interesting and eye-catching applications of AuNPs in nanomedicine and electronics. In this aspect, the importance of gold nanospheres cannot be neglected as it is more potent and advanced than other metallic NPs [1]. Phytomedicines are moving from fringe to a major stream and are used by greater number of people who seek remedies for health, with no or low side effects. In the recent era, a green route has emerged for NP fabrication, and people from both developing and developed countries have paid considerable attention to the eco-friendly and bio-friendly plant-based products in curing and preventing various human diseases [2]. Nano biotechnology is a new frontier for medicine with the application of nano-sized material for targeted cell or tissue-specific clinical intervention. Nanotechnology designed and employed techniques for the synthesis of systems that can interact at molecular (subcellular) level with great specificity in order to achieve maximum therapeutic potency with minimal side effects. The toxic chemicals limit the biomedical applications of chemically synthesized NPs [3]. The use of gold in nanostructure has become an attractive area of research during last several years because of its diverse applications in various fields of science and technology [4]. A great deal of efforts has been employed for the biological

* **Corresponding author: Sumaira Shah,** Department of Botany, Bacha Khan University Charsadda, Charsadda, KPK, Pakistan, e-mail: sunehra23@gmail.com
Rehman Ullah, Zahir Muhammad, Tauheed ul Haq: Department of Botany, University of Peshawar, Peshawar, KPK, Pakistan
Sajjad Ali Shah, Shah Faisal: Department of Biotechnology, Bacha Khan University Charsadda, Charsadda, KPK, Pakistan
Umbreen Khattak: Department of Botany, Islamia College University, University of Peshawar, Peshawar, KPK, Pakistan
Muhammad Taj Akbar: Department of Microbiology, Abdul Wali Khan University Mardan, Mardan, KPK, Pakistan

application of AuNPs in drug delivery, bio-diagnostics, biotechnology, and medicine as metallic gold is biologically nonreactive [5]. AuNPs have excellent antimicrobial activities against a wide of range of microorganisms such as bacteria and fungi [6]. These days AuNPs are used widely in chemical catalysis, nonlinear optics, surface-enhanced Raman scattering, nanoelectronics, gene expression, disease diagnosis, targeted drug delivery, and a controlled release of a drug at the desired site [7]. Similarly, nanoscale particles of gold also caught distinct position in biosensing, enzyme electrodes, catalysis electronics, super conductors, and cancer therapy [8]. The AuNPs prove overwhelming photocatalytic and therapeutic properties and are more effective against microbes [9].

Both *Euphorbia wallichii* shoot extract (SE) and AuNPs possess some novel physiological and physiochemical features such as electromagnetic and thermal conductance, intense plasmon resonance, biochemical stability, catalytic potential, antimicrobial activity, anti-HIV, antiangiogenic agents, antiarthritic, and antimalarial activities [10]. The current study is designed to biosynthesize AuNPs from *E. wallichii* SE and eluate its antimicrobial and other *in vivo* and *in vitro* applications.

2 Materials and methods

2.1 Plant collection and preparation of extract

E. wallichii shoots is collected from various localities of Khyber Pakhtunkhwa, Pakistan. The plant is identified at the Department of Botany University of Peshawar, Pakistan. A specimen of the collected plant is submitted to herbarium with voucher No. Bot. 20210 (UOP). The shoots are separated and washed with distilled water and dried for 1 week in shade. The dry shoots are powdered using an electric grinder. The shoot powder of 500 g is soaked in 1,500 mL ethanol for 2 weeks. The extract is filtered through Whatman filter paper and then evaporated at 40°C through a rotatory evaporator. The solid product is preserved at 4°C in refrigerator for NP synthesis.

2.2 Biosynthesis of AuNPs

The synthesis of AuNPs involved the mixing of 1 mL SE solution with 1 mM aqueous solution of $HAuCl_4$ in different ratios (1:1 to 1:5) by volume and stirred for 30 min at 35 ± 3°C till the color of the reaction mixture changes from pale yellowish to ruby red. After the completion of reaction, the AuNPs is centrifuged and washed with deionized water through centrifugation. The AuNPs were dried through freeze-drying technique. The synthesized AuNPs were then stored for further use.

2.3 Characterizations

The reduction of Au ions was confirmed by analyzing through UV-visible (UV-Vis) spectroscopic analysis of the synthesized mixture run against ethanol mixture and distilled water as a blank. The analysis is carrying out using UV-Vis spectrophotometer at a resolution of 1 nm from 300 to 800 nm. For further characterizations, the selected sample is freeze-dried.

Perkin Elmer spectrometer is used for FT-IR analysis in the range of 4,000–0 cm^{-1} at a resolution of 4 cm^{-1}. Thin pellets of KBr are prepared by pressing with the hydraulic pellet press and the sample was put on KBr pellet, which is then subjected to FTIR analysis. After FTIR analysis, the AuNP solution was dried at 90°C for XRD analysis using JEOL JDX-3532 X-ray diffractometer (JDX-3532, JEOL, Japan). The average particle size of AuNPs is calculated from the XRD pattern according to the full width at half maximum (FWHM) of the maximum intensity reflection peak. The size of NPs is calculated through the Scherrer's equation (Eq. 1).

$$D = \frac{K\lambda}{\beta_{\frac{1}{2}} \cos\theta} \times 100 \tag{1}$$

where D is the average crystal size, K = 0.89 is the Scherrer coefficient, λ = 1.5406 Å is the X-ray wavelength, 2θ is the Bragg's angle, β (β = sample, β reference) is FWHM in radians.

Surface morphology of AuNPs is inspected by using FE-SEM. A dried sample of AuNPs is coated on a carbon tape and then with gold before subjecting it to Spi-module sputter coater for analysis.

The distribution of AuNPs is evident from the TEM image. The synthesized AuNPs is used for the analysis of particle size. Specimens for TEM analysis are prepared by adding 1 or 2 drops of AuNPs solution onto the copper grids and allowing to dry at normal temperature. TEM (Philips Tacna G2 FEI F12, Brown University, Rhode Island, USA) is used to evaluate the surface morphology and size of NPs. The particles are washed and isolated by centrifugation method by taking 30 mL of suspension in distilled water containing AuNPs for 30 min at 12,000 rpm. The pellets are collected and dried at 50°C in the oven to

remove the rest of the water. The collected sample is used for EDX analysis. AuNPs are dried and drop coated on to the carbon film. EDX analysis is then carried out by using SEM equipped with a thermo EDX attachment.

2.4 *In vitro* bioassay

For bactericidal examination, Mueller–Hinton agar was poured in sterile petri plates and sterilized in autoclave. Freshly prepared diluted culture of the tested bacterial strains was swabbed on Mueller–Hinton agar plates. Wells of 6 mm diameters were bored, filled with 2 mg/mL each of streptomycin root extract (RE) and RE-mediated AuNPs, incubated at 30°C for 24 h, and evaluated for the zone of inhibition (mm) for antibacterial activity.

Antileishmanial bioassay was investigated against *Leishmania tropica* (KWH_{23}). From the standardized promastigotes' suspension (4×10^6 parasites/mL), 200 µL M-199 medium/well with 1×10^5 promastigotes were transferred to 96 well plates and fed with 10, 50, and 100 µg/mL of each of SE and AuNPs, incubated at 26°C for 48 h, and the number of promastigotes was counted with the help of Neubauer hemocytometer in microscope.

2,2-diphenyl-1-picrylhydrazyl (DPPH) scavenging activity was evaluated for both SE and AuNPs by mixing of 0.1 mM DPPH in methanol with different grades (10, 20, 40, 60, 80, and 100 µg/mL) of SE, AuNPs, and ascorbic acid and incubated for 90 min in dark. The absorbance for each run was measured at 517 nm at a difference of 30 min intervals (30, 60, and 90 min of incubation). Antioxidant potential was measured using (Eq. 2).

$$\% \text{ Antioxidant potential} = \frac{\text{Absorbance of control (nm)} - \text{Absorbance of test (nm)}}{\text{Absorbance of control (nm)}} \times 100 \quad (2)$$

2.5 *In vivo* bioassay

Analgesic potency was determined using Eddy's hot plate in Swiss albino mice. Animals were divided into five groups of six animals each, respectively, and received normal saline (10 mL/kg bw), diclofenac sodium (10 mg/kg bw), 50 mg/kg bw of each SE and AuNPs (ip), 100 mg/kg bw of SE and AuNPs (ip), and 200 mg/kg bw of each SE and AuNPs (ip). Animals response, i.e., paws flick or/and jumping to high temperature (55 ± 2°C), was investigated.

For antispasmodic activity, forenight fasted groups of mice were fed with normal saline (10 mL/kg bw), atropine sulfate (10 mg/kg bw), 50 mg/kg bw of each SE and AuNPs (po), 100 mg/kg bw of SE and AuNPs (po), and 200 mg/kg bw of each SE and AuNPs (po). After 15 min, the animals were fed with 0.2 mL of activated charcoal, sacrificed (after 30 min), dissected, and the intestine was cut down from pyloric to cecum. The distance traveled by the charcoal relative to the total intestinal length was measured as percentage of propulsion.

3 Results and discussion

3.1 Synthesis and characterizations of AuNPs

SE of *E. wallichii* acts as both a reducing agent and stabilizing agent. Reduction of Au^{3+} in the aqueous solution of $HAuCl_4$ was indicated by a change in color of reaction mixture from light pale to dark purple (Figure 1). *E. wallichii* possesses primary and secondary metabolites such as flavonoids, sugars, polyphenols, etc. which could be attributed to the reduction of gold ions to AuNPs [11]. The possible chemical equation for the synthesis of AuNPs will be:

$$HAuCl_{4(aq)} + SE_{(aq)} \rightarrow AuNPs \quad (3)$$

SE-mediated AuNPs were confirmed through UV-Vis spectroscopy. The UV-Vis spectra (Figure 2) showed surface plasmon resonance (SPR) band of between 500 and 600 nm, which is characteristic to nanogold particles. The obvious peak was found at about 548 nm for all ratios, where the maximum absorption was recorded at 1:2. Narrow sharp peak for gold revealed that the AuNPs are spheroidal in shape, small in size, and poly dispersed

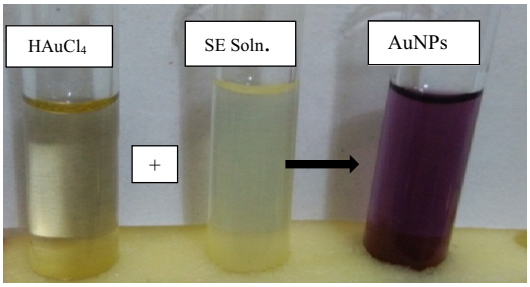

Figure 1: Synthesis of AuNPs through green approach using $HAuCl_4$ as a source of Au^{3+} and SE as the reducing and stabilizing agents.

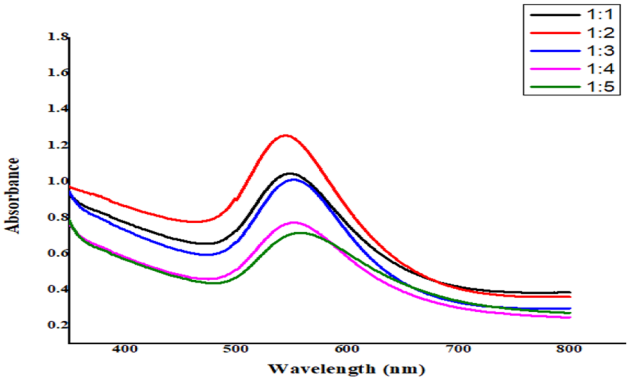

Figure 2: UV-Vis spectra of shoot extract (SE)-mediated AuNPs.

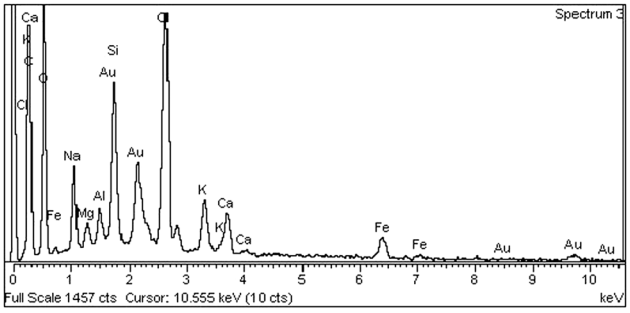

Figure 4: SEM and EDX spectra of SE-mediated AuNPs showing the optical density of metallic gold.

with no aggregation. As the particle size increases, the plasmon band frequency decreases and the band shifts to longer wavelength. The broader peaks with low intensities at other $HAuCl_4$ to SE ratios might be due to the relatively large anisotropic gold nanocrystals. Plasmon vibration on gold nanosurface produces SPR band centered at about 536 nm, giving the purplish aqueous medium. The SPR absorbance is strongly correlated to the shape, nature, and size of the NPs and their interparticular space [12,13].

The SEM micrographs (Figure 3a) revealed spherical morphology having intense agglomerated pattern of distribution. AuNPs have diverse size distribution, ranging from 28 to 200 nm. Transmission electron micrography represents well-dispersed Au-NPs encapsulated by SE matrix (Figure 3a). The SE matrix acts as the capping agent responsible for the stability of Au-NPs. The mean size of the Au-NPs was 17.52 ± 6.81 nm with predominantly spherical morphology. Moreover, different workers while using SEM and TEM reported phytogenic nanogold particles with spherical to triangular morphology with a size range of 10–300 nm [14].

The EDX spot -profile of SE-mediated Au-NPs shows signals of the Au atoms at 1.7, 8.5, 9.9, and 10.4 keV. The EDX spectra (shown in Figure 4) highlight the strongest optical absorption peak for gold (Au) at 2.1 keV, which is characteristic of Au. The multiple strong signals of chlorine (Cl) are due to the chloride salt of gold ($HAuCl_4$) used for the synthesis of AuNPs. Similar results were reported earlier, where energy dispersive X-ray spectroscopy (EDS) spectrum showed strong signal of Au at 2.0 and 2.1 keV for *coriander* leaf-mediated AuNPs [15], *barbated skull cup* extract-mediated AuNPs [16], and for AuNPs in *Mentha piperita* extract [17].

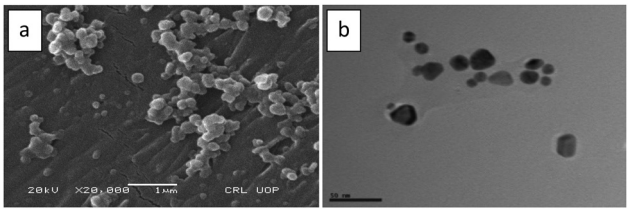

Figure 3: Electron microscopy of SE-mediated AuNPs: (a) scanning electron micrograph and (b) transmission electron micrograph.

Dynamic light scattering (DLS) analysis of AuNPs showing a trimodal size distribution curve (Figure 5), representing polydisperse mixture of AuNPs with a range of particulate diameter from 2.5 to 103.2 nm of 63.18 nm mean diameter. DLS showed comparatively larger diameter for the synthesized NPs than that shown in the SEM and TEM images, revealing an average particle of diameter 17.52 nm, which is due to the fact that SEM and TEM consider only the geometrical diameter of the metallic core while DLS analysis includes the ligand shell and determines the hydrodynamic size. Optical approaches for size measurements are restricted to the detection of particles with size larger than ~10 nm, whereas particles ranging from 1 to 8 nm can only be detected using the DLS approach [18].

The X-ray crystallography of biomimetic nanogold particles (Figure 6) showed multiple intense peaks at $2\theta = 16.84°$, 38.14°, 44.56°, 64.28°, and 78.00°. The intense peaks at 2θ values of 38.14°, 44.56°, 64.28°, and 78.00° correspond to (111), (200), (220), and (311) planes of Bragg reflections, representing crystalline nature with the face center cubic dimension of SE-mediated Au-NPs and matching the XRD pattern of pure Au-NPs with the database; JCPDS file number 00-004-0784 [19]. The other peaks represent crystalline amorphous phase of the organic matter adsorbed at the surface of AuNPs. The Debye–Scherrer's equation was used to calculate the crystallite size of the AuNPs on the basis of the FWHM of the (111) Bragg's reflection arising from the diffractogram, which showed the crystallite particle size to be about 21 nm.

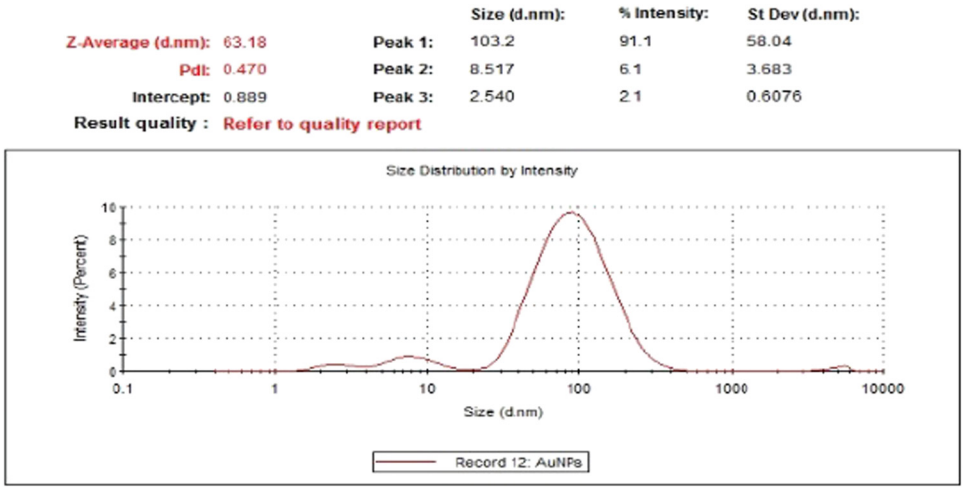

Figure 5: DLS graph showing size distribution, mean size, and standard deviation of SE-mediated AuNPs.

Comparative IR spectral analysis (Figure 7) of SE and SE-mediated AuNPs confirms the potential functional groups of SE responsible for the reduction of gold ions to AuNPs. In the current work, different vibrational stretches were reported at 3,240, 2,922, 2,340, 1,610, 1,507, 1,305, 1,220, and 1,016 wave numbers cm^{-1}, respectively, representing O–H stretch, H–bonded (alcohol/phenols), C–H stretch, C≡N stretch, C═O stretch, N–H bend (1° amines), C–N stretch (aliphatic amines), and C–O stretch (alcohol/carboxylic acids/esters/ethers). Vibrational wave number of 1,930 cm^{-1} present in SE represent C═O stretch of aldehyde characteristics of glycosides and carbohydrates masked at IR spectra of AuNPs, showing the potential functional group involved in the reduction of Au^{3+} to AuNPs. Some deep peaks were recorded in range of 1,500–1,000 cm^{-1}, which showed the presence of phosphate II and carbohydrates. Based on the available literature, it is evident that shifts in peak position in AuNPs IR spectra are due to the overchapping of these functional groups on the surface of metallic gold [20–23].

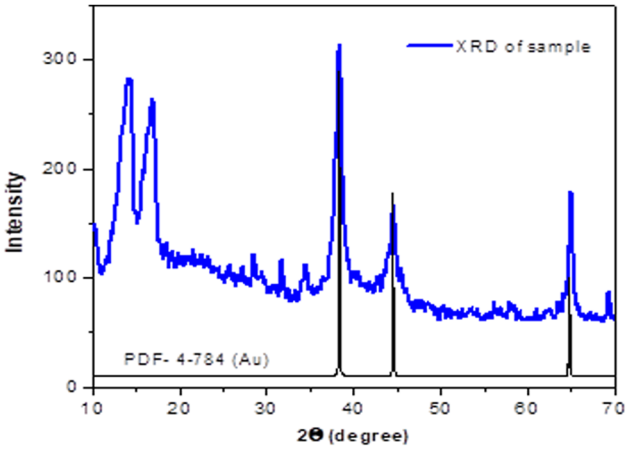

Figure 6: X-ray diffractogram of SE-AuNPs. The standard diffraction pattern of Au (JCPDS PDF no. 4-784) is also shown at the bottom.

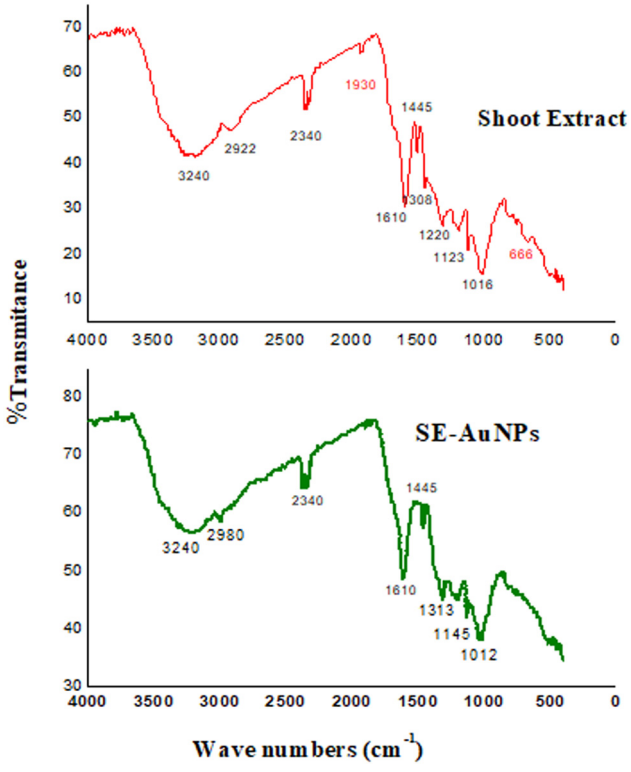

Figure 7: Comparative IR spectra of SE and SE-mediated AuNPs showing transmittance levels at different wavenumbers representing stretches of various functional groups.

3.2 Pharmacology

3.2.1 Analgesic activity

Analgesic response of mice to SE-mediated AuNPs is shown in Figure 8. At 30 min of drug administration, mice fed with 50, 100, and 200 mg/kg bw of SE-mediated AuNPs showed increase in latency time by 88.91%, 85.10%, and 82.25% (as percentage of diclofenac-Na), respectively. Mice fed with 50, 100, and 200 mg/kg bw of AuNPs acquired analgesia of 54.21%, 82.60%, and 86.53% as compared to absolute (100%) analgesia produced by diclofenac-Na at 60 min of dose administration. Similar trend in response of mice in terms of paw flick latency time was observed after 90 min of drug administration. Tissue damage more often causes pain by stimulating the nociceptive receptors but may also occur due to damages in the neural structures without nociception (neuralgia or neuropathic pain). The former responds easily to analgesics but often acute, while neuralgia is long-lasting and very difficult to treat as it persists long after healing the initial injury [24,25]. Opiate, serotonergic, and dopaminergic descending noradrenergics are central systems, modulating pain by complex processes while peripheral nociceptive mechanism involves synthesis of bradykinin, serotonin, histamine, leukotrienes, prostaglandins, and other endogenous substances. Thermal nociception may be prompted through opioid receptors or through inflection of several neurotransmitters involved in the relevant phenomena [26]. In the paw flick test, pre-oral administration of SE and SE-mediated AuNPs caused evident dose-related analgesia, though less analgesic than the standard diclofenac sodium. AuNPs were more potent and had crude extract probably due to their rapid diffusion as they are of considerably small sizes (1–100 nm). The current result suggests the involvement of μ-opioid receptors mediated by SE and AuNPs, resulting in the generation of analgesic response through the central system. Thermal nociceptive tests are more sensitive to opioid μ-agonists and nonthermal tests to opioid κ-agonists. In the thermal nociceptive tests, the animal response is typically integrated at the lower levels in CNS, thus, giving knowledge about the pain threshold, and could be used to test both narcotic and nonnarcotic analgesics [27]. The analgesic activity of *E. wallichii* is attributable to the presence of potent secondary metabolites, i.e., alkaloids, flavonoids, saponins, etc. The analgesic potential of some of the natural products has been attributed to their alkaloidal fraction. Flavonoids are also known for trigging prostaglandins responsible for peripheral nociceptive perception [28–30]. Similarly, saponins and tannins have been reported to possess anti-inflammatory and antinociceptive efficacy, where saponins inhibit histamine release [31–33].

3.2.2 Antispasmolytic activity

A dose-dependent gastrointestinal (GI) propulsion inhibition was observed for both atropine and SE-mediated AuNPs (Figure 9). Mean GI propulsion (percent) shown by mice fed normal saline was 72.27%. Maximum inhibition of GI propulsion (58.20%) was observed in mice treated with atropine sulfate (standard drug). The AuNPs at 50, 100, and 200 mg/kg bw showed 36.36%, 52.39%, and 69.05% antispasmodic potential compared to the standard drug (atropine) by inhibiting the muscular contraction by 21.16%, 30.49%, and 40.19%, respectively. GI lining is innervated by sympathetic and parasympathetic fibers chiefly associated with adrenergic and cholinergic fibers, respectively. The GI tract motility is mainly initiated by the local reflexes and is myogenic, and the extrinsic nerves of

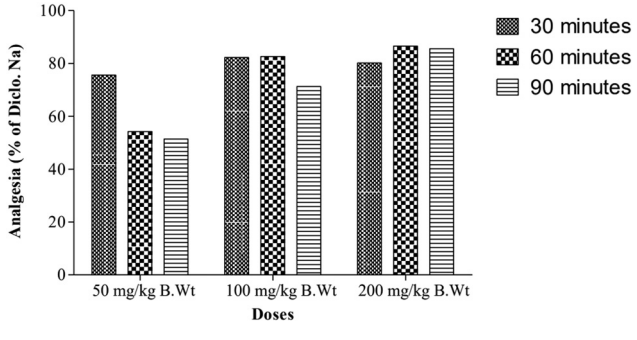

Figure 8: Analgesic efficacy of SE-mediated AuNPs, showing analgesia (percentage of diclofenac-Na) under different dose concentrations and time durations.

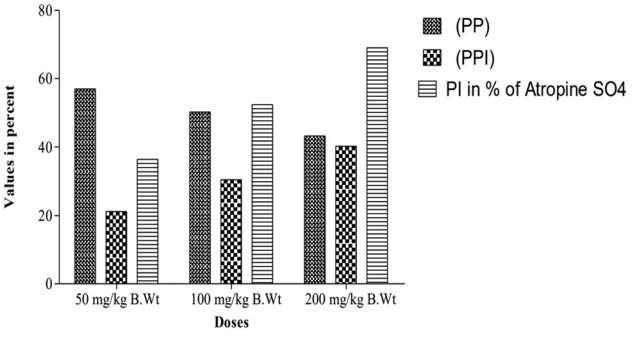

Figure 9: Spasmolytic efficacy of SE-mediated AuNPs, showing GI propulsion inhibition under different dose concentrations.

GI tract have limited role in modulating the peristalsis [34]. Opioid delays gastric emptying through acting on GI sphincters and hence decrease intestinal transit. The smooth muscles showing marked contraction when exposed to neurotransmitter acetylcholine released from acetylcholine receptors (parasympathetic nerves) [35]. Antispasmodics such as atropine and dicyclomine are antagonists of muscarinic acetylcholine receptors. Extract derived from shoot of *E. wallichii* and its mediated AuNPs exhibited promising antispasmodic effect most probably by antagonizing muscarinic acetylcholine receptors. The spasmolytic effect of NPs was more evident than extracts alone due to the provision of large surface area for antagonism because of larger size to mass ratio. The blockage of muscarinic acetylcholine receptor is coupled with the decline in intestinal motility hence lessening the excretion of water and electrolytes [36].

3.2.3 Antioxidant activity

Antioxidant efficacy of SE-mediated AuNPs was assessed by measuring its bleaching potential on DPPH. AuNPs exhibits time- and dose-dependent effectiveness. The EC50s for ascorbate (the standard drug used) were 3.46, 2.86, and 1.64 µg/mL at 30, 60, and 90 min of reaction time, respectively. AuNPs showing effective concentration for 50% DPPH inhibition at 30, 60, and 90 min of reaction time were 31.52, 18.29, and 15.32 µg/mL, respectively (Figure 10). DPPH scavenging assay is considered as the model for lipophilic-free radicals, which is initiated by auto-oxidation of lipids. Phytometabolites have the tendency to donate hydrogen (reduction) to DPPH (ROS) which is indicated by its bleaching purple color, where the degree of discoloration is correlated with the concentration and potential of antioxidants [37]. The natural compound-mediated AuNPs has redox properties against free radicals, decomposing the peroxides or slaking singlet and triplet oxygen or decomposing peroxides. The current study represents moderate antioxidant efficacy of SE-mediated AuNPs due to the utilization of redox potentials of phytometabolites in SE during the synthesis of AuNPs as evident in the FTIR analysis. The synthesis of AuNPs and antioxidant activity are competing processes where both are dependent on the concentrations and potential of reducing phytochemicals. Researchers studied the antioxidant potential of metallic NPs by evaluating longan fruit juice. The synthesized NPs of longan fruit juice showed significant DPPH free radical scavenging activity [38]. Our current results are in line with the findings of these researchers.

3.2.4 Antileishmanial activity

The antileishmanial efficacy of SE-mediated AuNPs was analyzed against the promastigote form of *L. tropica*. Both SE and AuNPs revealed dose-dependent antipromastigote efficacy by recording 44%, 52%, and 71% mortality at 10, 50, and 100 µg/mL, respectively. LD_{50}, LD_{70}, and LD_{90} values recorded were 13.86, 49.42, and 310.56 µg/mL (Table 1). Though both promastigote and amastigote forms show remarkable differences but still similar in their metabolic pathways and hence the target against the promastigote could be relevant against the amastigote [39]. Metal NPs show the tendency to impair with glycoprotein 63 and lipophosphoglycan found on the leishmanial parasite surface and are responsible for infection. NPs often release core metal ion, generate ROS, and inhibit the growth of *Leshmania* by degenerating its cytochemical profile [40]. Similarly, AuNPs enhance antileishmanial activity in contrast to micro materials. The investigation on gold $[Au(dppz)_2]Cl_3$ complex showed that the gold-derived NPs exhibit significant dose-dependent antipromastigote activity against *Leishmania mexicana* [41,42].

3.2.5 Antifungal activity

Both SE and SE-mediated AuNPs presented variable antifungal activities against the studied pathogenic fungal strains. *Fusarium solani* was the most resistive fungus because it showed no inhibition for both SE and AuNPs (Figure 11). *Aspergillus niger* was markedly susceptible by showing 61.53 ± 0.88% and 70.85 ± 1.57% of mycelia growth inhibition to SE and AuNPs, respectively. SE and AuNPs induced mycelia growth inhibition by 31.74 ± 0.22% and 54.22 ± 0.48% against *Candida albicans*, 48.75 ± 0.49% and 55.67 ± 0.50% against *Aspergillus flavus*, and 17.22 ± 0.11% and 37.60 ± 1.08% against *Aspergillus parasiticus*, respectively. The SE-mediated AuNPs exhibited alleviated antifungal activity compared to SE due to its large surface area and small size. Available literature revealed that the antifungal efficacy of AuNPs depends on the size, shape, concentration, and nature of surfactants used [43]. It is reported that AuNPs restrict the transmembrane H^+ efflux by inhibiting H^+-ATPase activity in a size-dependent manner [44].

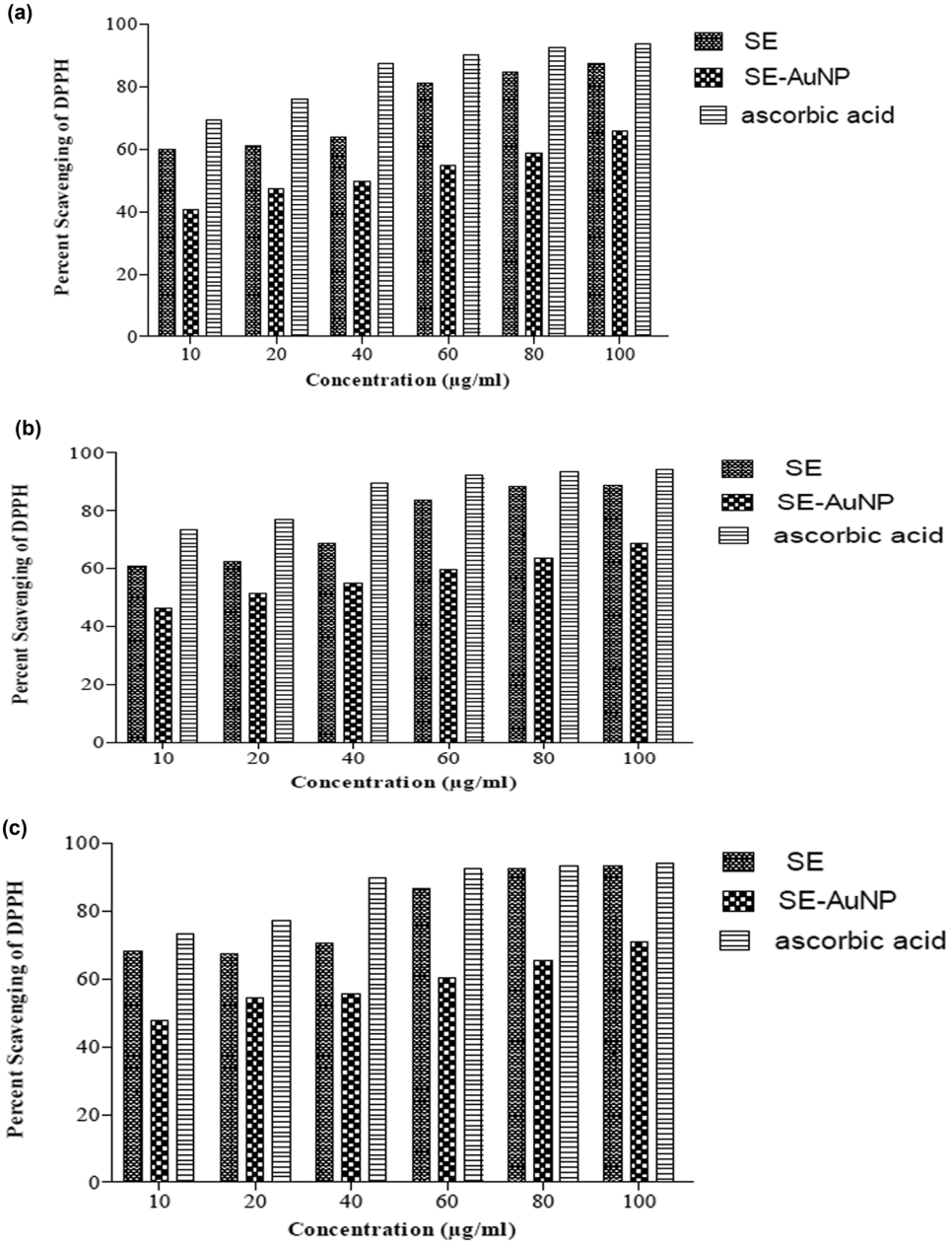

Figure 10: DPPH radical scavenging activity of SE, SE-mediated AuNPs, and ascorbic acid (standard) under different concentrations at (a) 30 min of incubation time, (b) 60 min of incubation time, and (c) 90 min of incubation time.

Table 1 The: efficacy of anti-promastigotes' various concentrations of SE-mediated AuNPs against *L. tropica*

Treatment	Doses (µg/mL)	No. of promastigotes (1×10^4)	% mortality	LC_{50}	LC_{50}	LC_{90}	Probit
Control DMSO	0.5%	100	—	—	—	—	—
AuNPs	10	56 ± 3.87	44	21.39	149.02	2468.11	$Y = 4.17 + 0.62X$
	50	48 ± 2.56	52				
	50	29 ± 3.09	71				

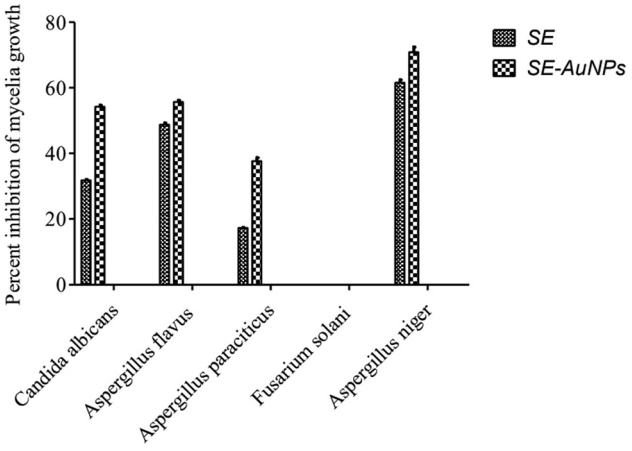

Figure 11: Fungicidal potency of SE and SE-mediated AuNPs against the different pathogenic fungal strains.

3.2.6 Antibacterial activity

Zones of inhibition corresponding to SE-mediated AuNPs against *Escherichia coli*, *Staphylococcus aureus*, *Bacillus pumilus*, *Pseudomonas aeruginosa*, and *Klebsiella pneumoniae* were 21.9 ± 0.5 mm, 15.2 ± 0.5 mm, 21.8 ± 0.4 mm, 17.7 ± 0.4 mm, and 17.3 ± 0.5 mm, respectively, thus exhibiting the antibacterial potency of 76.31%, 68.47%, 79.85%, 48.10%, and 65.53%, respectively (Figure 12). Generally, gram-negative strains show more susceptibility than gram-positive strains because of a thicker peptidoglycan layer in the gram-positive than the gram-negative bacteria; thus, comparatively larger doses of NPs are required for the former strains [45]. The possible mechanism for bacterial growth inhibition by AuNPs is either altering the membrane potential for ATP synthesis or/and declining the tRNA binding capacity for ribosome,

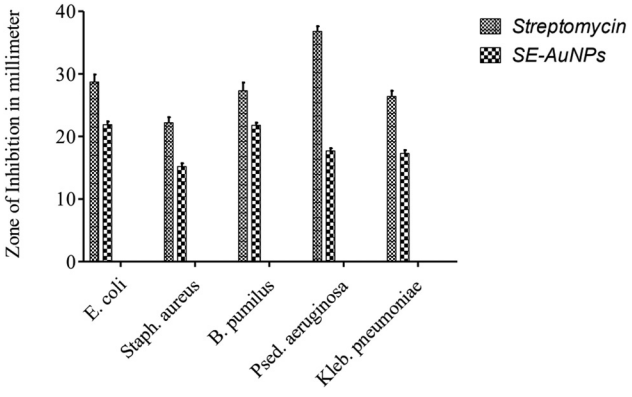

Figure 12: Antibacterial potency of SE-mediated AuNPs in comparison with the standard streptomycin against different pathogenic fungal strains.

thus disordering its protein synthetic mechanism [46]. The pronounced antibacterial potency of AuNPs is due to its small size and large surface area which facilitates rapid diffusion and enhances the contact area, interacting with microbes. Bacterial DNA and membrane proteins are altered as a first choice for AuNPs, by binding to their phosphoric and thiol groups, respectively, thus inhibiting bacterial growth. Most of the research articles report the synthesized NPs to be active against bacteria and fungus. The metallic NPs have significant result against different bacterial strains such as *E. coli*, *Bacillus subtilis*, *K pneumoniae*, and *Pseudomonas fluorescens* and fungal strains such as *Trichophyton simii*, *Trichophyton mentagrophytes*, and *Trichophyton rubrum* [47]. *Aloe vera* leaf extract NPs were evaluated against different strains of *S. aureus* and *E. coli* bacteria. The inhibition zone for *S. aureus* (12 mm) was higher than that of *E. coli* (around 10 mm) [48]. Therefore, our current results are in consistency with the findings of these researchers.

4 Conclusion

Fabrication of gold nanocrystals has been carried out using the reducing power of *E. wallichii* SE. Spectroscopic, morphologic, and structural analyses suggest the key role of phytochemicals of *E. wallichii* in eco-friendly phytofabrication of polydisperse, crystalline and spherical nanogold particles. *In vitro* and *in vivo* pharmacologies strongly support the use of surface functionalized AuNPs of plant origin as analgesic because the alkaloids, flavonoids, and saponins of *E. wallichii* trigger prostaglandins responsible for peripheral nociceptive perception. The spasmolytic effect of NPs was more evident than extracts alone due to the provision of large surface area for antagonism because of larger size to mass ratio. The antioxidant potential of AuNPs has redox properties against free radicals and represents moderate antioxidant efficacy due to the utilization of redox potentials of phytometabolites in the synthesis of AuNPs. The antimicrobial agent is alternative to the conventional phytomedicine due to its cost-efficient, eco-friendly, and alleviated therapeutic potential.

Acknowledgments: Authors are grateful to Centralized Resource Laboratory (CRL) University of Peshawar, Pakistan for providing SEM, EDX, XRD, etc. facilities. National Institution of Health (NIH) Islamabad is acknowledged with thanks for provision of experimental animals.

Research funding: Authors state no funding involved.

Author contributions: Rehman Ullah, Zahir Muhammad, and Sajjad Ali Shah conceptualized and performed the experiments; Sumaira Shah wrote the manuscript and provided chemical reagents; Shah Faisal performed formal analysis and characterized the nanoparticles; Umbreen Khattak, Tauheed ul Haq, and Taj Akbar helped in SD analysis.

Conflict of interest: Authors state no conflict of interest.

References

[1] Eskandari-Nojehdehi M, Hoda JM, Javad RS. Optimization of processing parameters in green synthesis of gold nanoparticles using microwave and edible mushroom (Agaricus bisporus) extract and evaluation of their antibacterial activity. Nanotechnol Rev. 2016;5(6):537–48.

[2] Khan ZH, Amjad K, Young MC, Noor SS, Arif UK, Nawshad M, et al. Enhanced antimicrobial, anti-oxidant applications of green synthesized AgNPs- an acute chronic toxicity study of phenolic azo dyes & study of materials surface using X-ray photoelectron spectroscopy. J Photochem Photobiol B Biol. 2018;180:208–17.

[3] Rahimirad A, Afshin J, Hamid M, Navideh A, Hoda JM. Biological approach in nanobiotechnology – screening of four food pathogenic bacteria extracts ability in extracellular biosynthesis of gold nanoparticles. Biologia. 2020;75(4):619–25.

[4] Iqbal J, Shah NS, Sayed M, Niazi NK, Imran M, Khan JA, et al. Nano-zerovalent manganese/biochar composite for the adsorptive and oxidative removal of Congo-red dye from aqueous solutions. J Hazard Mater. 2021;403:123854.

[5] Khan ZH, Shah NS, Iqbal J, Khan AU, Imran M, Alshehri SM, et al. Biomedical and photocatalytic applications of biosynthesized silver nanoparticles: ecotoxicology study of brilliant green dye and its mechanistic degradation pathways. J Mol Liq. 2020;319:114114.

[6] Shams S, Khan AU, Yuan Q, Ahmed W, Wei Y, Khan ZH, et al. Facile and eco-benign synthesis of Au@ Fe_2O_3 nanocomposite: efficient photocatalytic, antibacterial and antioxidant agent. J Photochem Photobiol B Biol. 2019;199:111632.

[7] Eskandari-Nojedehi M, Hoda JM, Javad RS. Hydrothermal green synthesis of gold nanoparticles using mushroom (*Agaricus bisporus*) extract: physico-chemical characteristics and antifungal activity studies. Green Processing and Synthesis. 2018;7:38–47.

[8] Sun Y, Xia Y. Increased sensitivity of surface Plasmon resonance of gold nanoshells compared to that of gold solid colloids in response to environmental changes. Anal Chem. 2002;74:5297–305.

[9] Abbasian R, Hoda JM. Green approach in gold, silver and selenium nanoparticles using coffee bean extract. Open Agric. 2020;5(1):761–7.

[10] Geddes CD, Parfenov A, Gryczynski I, Lakowicz JR. Luminescent blinking of gold nanoparticles. Chem Phys Lett. 2003;380:269–72.

[11] Ambreen M, Ali S, Muhammad Z, Muhammad A. *Euphorbia wallichii* and *Oxyria digyna*: valuable Antioxidant Sources. Biologia (Pak). 2014;60(2):249–53.

[12] Shah R, Sajjad AS, Sumaira S, Shah F, Farhan U. Green synthesis and antibacterial activity of gold nanoparticles of *Digera muricata*. Indian J Pharm Sci. 2020;82(2):374–8.

[13] Eustis S, El-Sayed MA. Why gold nanoparticles are more precious than pretty gold: noble metal surface plasmon resonance and its enhancement of the radiative and nonradiative properties of nanocrystals of different shapes. Chem Soc Rev. 2006;35:209–17.

[14] Philip D. Rapid green synthesis of spherical gold nanoparticles using *Mangifera indica* leaf. Spectrochim Acta Part A Mol Biomol Spectrosc. 2010;77(4):807–10.

[15] Narayanan KB, Sakthivel N. Biosynthesis of gold nanoparticles by using *coriander* leaf extract. Mater Lett. 2008;62:4588–90.

[16] Wang Y, Xiaxiao H, Kemin W, Xiorong Z, Weihong T. Synthesis of gold nanoparticles using *Barbated skull cup herb* extract and its primary application in electrochemistry. Colloids Surf B. 2009;73:75–9.

[17] Ali DM, Thajuddin N, Jeganathanb K, Gunasekaranc M. Plant extract mediated synthesis of silver and gold nanoparticles and its antibacterial activity against clinically isolated pathogens. Colloids Surf B. 2011;85:360–5.

[18] Elia P, Zach R, Hazan S, Kolusheva S, Porat Z, Zeiri Y. Green synthesis of gold nanoparticles using plant extracts as reducing agents. Int J Nanomed. 2014;9:4007–21.

[19] Anuradha J, Abbasi T, Abbasi SA. An eco-friendly method of synthesizing gold nanoparticles using an otherwise worthless weed pistia (*Pistia stratiotes* L.). J Adv Res. 2015;6(5):711–20.

[20] Annamalai A, Babu ST, Jose NA, Sudha D, Lyza CV. Biosynthesis and characterization of silver and gold nanoparticles using aqueous leaf extraction of Phyllanthus amarus Schum and Thonn. World ApplSci J. 2011;13:1833–40.

[21] Naiya TK, Singha B, Das SK. FTIR study for the Cr (VI) removal from aqueous solution using rice waste. Int Proc Chem Biol Environ Eng. 2011;10:114–9.

[22] Shi W, Sahoo Y, Swihart MT. Gold nanoparticles surface-terminated with bifunctional ligands. Colloids Surf A Physicochem Eng Asp. 2004;246(1):109–13.

[23] Shah F, Sajjad AS, Sumaira S, Muhammad TA, Faheem J, Ihteshamul H, et al. *In vitro* biomedical and photo-catalytic application of bio-inspired *Zingiber officinale* mediated silver nanoparticles. J Biomed Nanotechnol. 2020;16:1–13.

[24] Juan H, Lembeck F. Action of peptides and other analgesic agents on paravascular pain receptors of the isolated perfused rabbit ear. Naunyn-Schmiedeberg's Arch Pharmacol. 1974;283:151.

[25] Somasundaram S, Sigthorsson G, Simpson RJ, Watts J, Jacob M, Tavares IA, et al. Uncoupling of intestinal mitochondrial oxidative phosphorylation and inhibition of cyclooxygenase are required for the development of NSAID- enteropathy in the rat. Aliment Pharmacol Ther. 2000;14(5):639.

[26] Mishra DG, Ghosh PS, Kumar, Panda PK. An experimental study of analgesic activity of selective COX-2 inhibitor with conventional NSAIDs. Asian J Pharm Clin Res. 2011;4(1):78–81.

[27] Furst S, Gyires K, Knoll J. Analgesic profile of rimazolium as compared to different classes of painkillers. Drug Res. 1988;4:552.
[28] Fernanda LB, Victor AK, Amelia TH, Elisabetsky E. Analgesic properties of umbellatine from *Psychotria umbellate*. Pharm Biol. 2002;44:54.
[29] Bittar M, Souza MM, Yunes RA, Lento R, Monache FD, Cechinel-Filho V. Antinociceptive activity of I3, II8-binaringenin: a biflavonoid present in plants of the guttiferae. Planta Med. 2000;66:84.
[30] Santa-Cecília FV, Vilela FC, Rocha CQ, Dias DF, Cavalcante GP, Freitas LAS, et al. Anti- inflammatory and antinociceptive effects of *Garcinia brasiliensis*. J Ethnopharmacol. 2011;133:467.
[31] Hosseinzadeh H, Younesi HH. Antinociceptive and anti-inflammatory effects of *Crocus sativus* L. stigma and petal extracts in mice. BMC Pharmacol. 2002;2:7. doi: 10.1186/1471-2210-2-7.
[32] Wang SY, Lan X, Xiao J, Yang J, Kao Y, Chang S. Anti inflammatory activity of *Linderaery throcarpa* fruits. Phytother Res. 2008;22:213–6.
[33] Das SC, Bhadra S, Roy S, Saha SK, Islam MS, Bachar SC. Analgesic and anti-inflammatory activities of ethanolic root extract of *Swertiachirata*(Gentianaceae). Jordan J Biol Sci. 2012;5(1):31–36.
[34] Shahriar M, Bhuiya MS, Khan MTH, Gafur MA, Choudhri MSK. Pharmacological study of *Symplocosra cemosa* Roxb. Ham Med. 2000;43:8–18.
[35] Ponarulselvam S, Panneerselvam C, Murugan K, Aarthi N, Kalimuthu K, Thangamani S. Synthesis of silver nanoparticles using leaves of *Catharanthus roseus* Linn. G. Don and their antiplasmodial activities. Asian Pac J Trop Biomed. 2012;2(7):574–80.
[36] Hajhashemi V, Sadraei H, Ghannadi AR, Mohseni M. Antispasmodic and antidiarrhoeal effect of *Saturejahortensis* L. essential oil. J Ethnopharmacol. 2000;71:187–92.
[37] Sumaira S, Siraj D, Adnan K, Rehmanullah, Sajjad AS. Green synthesis and antioxidant study of silver nanoparticles of root extract of *Sageretia thea* and its role in oxidation protection technology. J Polym Environ. 2017;26(2):2323–32.
[38] Khan AU, Wei Y, Ahmad A, Khan ZH, Tahir K, Khan SU, et al. Enzymatic browning reduction in white cabbage, potent antibacterial and antioxidant activities of biogenic silver nanoparticles. J Mol Liq. 2016;215:39–46.
[39] Mougneau E, Bihl F, Glaichenhaus N. Cell biology and immunology of leishmania. Immunol Rev. 2011;240(1):286–96.
[40] Allahverdiyev AM, Abamor ES, Bagirova M, Ustundag CB, Kaya C, Kaya F, et al. Antileishmanial effect of silver nanoparticles and their enhanced antiparasitic activity under ultraviolet light. Int J Nanomed. 2011;6:2705–14.
[41] Faisal S, Khan MA, Jan H, Shah SA, Shah S, Rizwan M, et al. Edible mushroom (*Flammulina velutipes*) as biosource for silver nanoparticles: from synthesis to diverse biomedical and environmental applications. Nanotechnology. 2021;5(32):6.
[42] Torabi N, Mohebali M, Shahverdi AR, Rezayat SM, Edrissian GH, Esmaeili J, et al. Nanogold for the treatment of zoonotic cutaneous leishmaniasis caused by leishmania major (MRHO/IR/75/ER): an animal trial with methanol extract of eucalyptus camaldulensis. JPSH. 2011;1(1):13–6.
[43] Ahmad T, Wani IA, Lone IH, Ganguly A, Manzoor N, Ahmad A, et al. Antifungal activity of gold nanoparticles prepared by solvothermal method. Mater Res Bull. 2013;48(1):12–20.
[44] Wani IA, Ahmad T. Size and shape dependent antifungal activity of gold nanoparticles: a case study of Candida. Collids Surf B. 2013;101:162–70.
[45] Umadevi M, Rani T, Balkrishnan T, Ramanibai R. Antimicrobial activity of silver nanoparticles under an ultrasonic field. Int J Pharm Sci Nanotechnol. 2011;4:1491–6.
[46] Cui Y, Zhao Y, Tian Y, Zhang W, Lü X, Jiang X. The molecular mechanism of action of bactericidal gold nanoparticles on *Escherichia coli*. Biomaterials. 2012;33:2327–33.
[47] Khan ZH, Khan A, Chen Y, Shah NS, Muhammad N, Khan AU, et al. Biomedical applications of green synthesized Nobel metal nanoparticles. J Photochem Photobiol B Biol. 2017;173:150–64.
[48] Fardsadegh B, Hoda JM. Aloe vera leaf extract mediated green synthesis of selenium nanoparticles and assessment of their *in vitro* antimicrobial activity against spoilage fungi and pathogenic bacteria strains. Green Process Synth. 2019;8(1):399–407.